JOURNAL OF AIRCRAFT
Vol. 35, No. 2, March–April 1998

Estimation of Wind from Airplane States in Coordinated Flight

Amnon Katz* and Manu Sharma†
University of Alabama, Tuscaloosa, Alabama 35487-0280

A filter is defined that extracts the wind aloft from the Earth velocity and the orientation of a flight vehicle in coordinated flight (data that are available in the context of distributed interactive simulation). A convergence theorem is proved stating that the estimated wind monotonically approaches the true wind when the latter is horizontal and constant. The filter builds the transverse component of the wind and converges to the full wind as the flight vehicle changes heading. The fastest convergence occurs when the filter is applied at heading intervals equal to a critical interval that depends on the bank.

I. Introduction

THE present paper develops a procedure for determining wind aloft from a history of Earth velocity (three dimensional) and orientation of a flight vehicle in coordinated flight. These data are readily available in the context of distributed interactive simulation (DIS).

The DIS technology, now codified in Institute of Electrical and Electronics Engineers standard 1278,[1] allows for the networking of a large number of simulators at diverse locations into a coherent virtual environment. Typically, each simulator computes the state of one vehicle, but displays any other vehicle that is within visual range. The states of such other vehicles are learned from data packets received periodically over the network and, in between packets, are extrapolated.

The DIS community has borrowed the classical navigation term *dead reckoning* to describe the process of extrapolating the state of a remotely simulated vehicle. Dead reckoning was initially introduced in DIS as a device for limiting network traffic. A sending simulator (the sender) would simulate the dead reckoning of a receiving simulator (the receiver). As long as the receiver's presentation error was within prescribed thresholds, no updates were transmitted.[2] It was later realized that, quite apart from bandwidth considerations, dead reckoning is crucial to reducing the error with which the states of remote vehicles are known. Even when updates are not withheld, dead reckoning is required to compensate for transmission delays and synchronization errors.[3,4]

Katz and Graham[5,6] developed methods of dead reckoning (K&G methods) based on the assumption that an airplane flies coordinated. The K&G airplane-specific extrapolation methods proved three to five times more accurate than generic methods. This meant that network traffic could be cut by a factor of three to five, or, in the alternative, the errors in presenting a remote player could be cut by the same factor.

Coordinated flight implies that an aircraft flies through the air along its plane of symmetry, rather than sideways. However, airplane states reported in DIS or obtained through telemetry reflect the motion of the aircraft relative to the ground rather than the air. Before the K&G extrapolation methods can be applied to full advantage, one must convert the Earth system velocity to the air system velocity. For that purpose, it is necessary to know the wind.

In the absence of a source for wind information, it is possible to extract that information from the airplane states themselves. This, again, relies on the assumption of coordinated flight. Any sideways motion that is detected is ascribed to wind. There is no way to extract the wind fully from the instantaneous state. Only the crosswind component can be estimated. However, over a period of time, with the airplane changing heading, the estimate can be refined until it is sufficiently accurate.

The present paper develops an iterative wind extraction filter. A convergence theorem is proved. Optimal strategies for applying the filter to the state history of a turning airplane are devised.

The DIS standard specifies that full six-degree-of-freedom (DOF) information about each vehicle be transmitted, which includes three-dimensional position, velocity, and acceleration, as well as three-DOF orientation and angular rates. The translational data are relative to the Earth. Wind information is not included. The present paper is tied to the DIS context through the assumption that Earth-system six-DOF data are available, whereas the wind is unknown. The variables of state actually used in the wind estimation process are velocity and orientation.

In simulation, the wind applied by each simulator is known, even if not included in the DIS packet. However, DIS applies to live as well as virtual simulation, that is, to aircraft flying through the air, simulating a war exercise, as well as to manned simulators. For live aircraft, obtaining accurate winds aloft is not trivial. At some future time DIS may be adopted for the air traffic control (ATC) environment, and civil airplanes may transmit DIS packets. At such time, the wind extraction algorithm of the present paper will be available to ATC.

Dead reckoning should be of value in other fields, e.g., ground-to-air and air-to-air gunnery, where it is necessary to extrapolate the position of a target over the period that a projectile is in transit. Applicability of the methods developed in the present paper and in Ref. 6 to these and other situations hinges upon availablity of the requisite state information for the target, in particular, orientation data.

II. Closed-Form Extraction of Transverse Wind

We start by laying out our assumptions and notation. There are a variety of air currents in the atmosphere. We address only steady wind, i.e., uniform horizontal motion of the airmass over a flat Earth. The wind velocity is assumed horizontal and constant over both space and time. This is a fair model of winds aloft above the turbulence level. While winds aloft do

Received Feb. 6, 1997; revision received Oct. 3, 1997; accepted for publication Oct. 3, 1997.

*Professor, Department of Aerospace Engineering and Mechanics, P.O. Box 870280.

†Graduate Student, Department of Aerospace Engineering and Mechanics; currently at Symsystems, 12508 E. Briarwood Avenue, Suite 1F, Englewood, CO 80112.

vary with altitude and change over time, these changes are small over the time periods and altitude ranges involved in normal aircraft maneuvers. The procedures we develop converge to the prevailing wind faster than it changes and, once converged, continue to produce the correct wind. The unknown constant wind is denoted $\boldsymbol{W}$.

We use an Earth fixed-coordinate system, with the x and y axes horizontal and z pointing down. The three unit vectors in the major directions of the Earth coordinate system are $\hat{\boldsymbol{\imath}}_e$, $\hat{\boldsymbol{\jmath}}_e$, $\hat{\boldsymbol{k}}_e$. The airplane velocity provided by the remote simulator or by telemetry is $\boldsymbol{V}$. The airplane state includes the body orientation. Regardless of the form in which this information is conveyed, it can be transformed into direction cosines, which, in turn, can be interpreted as the Earth-system components of the three unit vectors in the major directions of the body coordinate system $\hat{\boldsymbol{\imath}}_b$, $\hat{\boldsymbol{\jmath}}_b$, $\hat{\boldsymbol{k}}_b$.

The body coordinates are a forward, right, down system. The x–z plane is the plane of symmetry of the airplane. We assume coordinated flight, which means that the air velocity $\boldsymbol{V}-\boldsymbol{W}$ is in the x–z plane. This implies

$$(\boldsymbol{V}-\boldsymbol{W})\cdot\hat{\boldsymbol{\jmath}}_b = 0 \tag{1}$$

The wind component along $\hat{\boldsymbol{\jmath}}_b$ can be determined as

$$\boldsymbol{W}\cdot\hat{\boldsymbol{\jmath}}_b = \boldsymbol{V}\cdot\hat{\boldsymbol{\jmath}}_b \tag{2}$$

In general, $\hat{\boldsymbol{\jmath}}_b$ is not horizontal, whereas the wind is. The unknown wind may be decomposed into a component in the x_b–z_b plane (the longitudinal wind) and another component perpendicular to the first (the transverse wind). We introduce unit vectors $\hat{\boldsymbol{e}}_L$ and $\hat{\boldsymbol{e}}_T$ in the direction of the longitudinal and transverse wind; $\hat{\boldsymbol{e}}_L$ and $\hat{\boldsymbol{e}}_T$ are both horizontal

$$\hat{\boldsymbol{e}}_L\cdot\hat{\boldsymbol{k}}_e = 0 \tag{3}$$

$$\hat{\boldsymbol{e}}_T\cdot\hat{\boldsymbol{k}}_e = 0 \tag{4}$$

and $\hat{\boldsymbol{e}}_L$ is in the body plane of symmetry

$$\hat{\boldsymbol{e}}_L\cdot\hat{\boldsymbol{\jmath}}_b = 0 \tag{5}$$

Equations (3) and (5) determine $\hat{\boldsymbol{e}}_L$ as

$$\hat{\boldsymbol{e}}_L = \frac{\hat{\boldsymbol{\jmath}}_b\times\hat{\boldsymbol{k}}_e}{|\hat{\boldsymbol{\jmath}}_b\times\hat{\boldsymbol{k}}_e|} \tag{6}$$

Then $\hat{\boldsymbol{e}}_T$ may be determined as

$$\hat{\boldsymbol{e}}_T = \hat{\boldsymbol{e}}_L\times\hat{\boldsymbol{k}}_e = \frac{(\hat{\boldsymbol{\jmath}}_b\times\hat{\boldsymbol{k}}_e)\times\hat{\boldsymbol{k}}_e}{|\hat{\boldsymbol{\jmath}}_b\times\hat{\boldsymbol{k}}_e|} = \frac{\hat{\boldsymbol{\jmath}}_b-(\hat{\boldsymbol{\jmath}}_b\cdot\hat{\boldsymbol{k}}_e)\hat{\boldsymbol{k}}_e}{|\hat{\boldsymbol{\jmath}}_b\times\hat{\boldsymbol{k}}_e|} = \frac{\boldsymbol{\jmath}_{bh}}{|\hat{\boldsymbol{\jmath}}_b\times\hat{\boldsymbol{k}}_e|} \tag{7}$$

where

$$\boldsymbol{\jmath}_{bh} \equiv \hat{\boldsymbol{\jmath}}_b-(\hat{\boldsymbol{\jmath}}_b\cdot\hat{\boldsymbol{k}}_e)\hat{\boldsymbol{k}}_e \tag{8}$$

is the horizontal component of $\hat{\boldsymbol{\jmath}}_b$ (Fig. 1).

The true wind may be expressed as

$$\boldsymbol{W} = W_L\hat{\boldsymbol{e}}_L + W_T\hat{\boldsymbol{e}}_T \tag{9}$$

Only the transverse wind contributes to Eq. (2) and only it can be estimated. Substituting Eq. (9) in Eq. (2), one finds

$$W_T\hat{\boldsymbol{e}}_T\cdot\hat{\boldsymbol{\jmath}}_b = \boldsymbol{V}\cdot\hat{\boldsymbol{\jmath}}_b \tag{10}$$

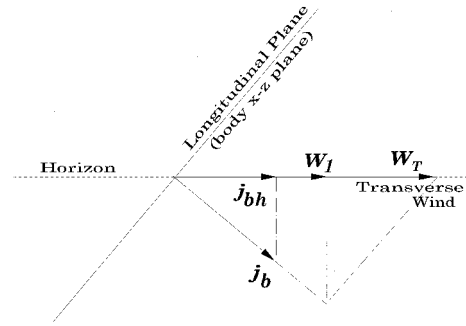

Fig. 1 Extraction of the transverse wind.

from which the W_T may be determined, and the wind estimated as

$$\boldsymbol{W}_1 = \frac{\boldsymbol{V}\cdot\hat{\boldsymbol{\jmath}}_b}{\hat{\boldsymbol{e}}_T\cdot\hat{\boldsymbol{\jmath}}_b}\hat{\boldsymbol{e}}_T = \frac{\boldsymbol{V}\cdot\hat{\boldsymbol{\jmath}}_b}{\boldsymbol{\jmath}_{bh}\cdot\hat{\boldsymbol{\jmath}}_b}\boldsymbol{\jmath}_{bh} = (\boldsymbol{V}\cdot\hat{\boldsymbol{\jmath}}_b)\frac{\boldsymbol{\jmath}_{bh}}{|\boldsymbol{\jmath}_{bh}|^2} \tag{11}$$

When the wings are level, $\boldsymbol{\jmath}_{bh} = \hat{\boldsymbol{\jmath}}_b$, and $|\boldsymbol{\jmath}_{bh}| = 1$. In general, $|\boldsymbol{\jmath}_{bh}|$ may be expressed as

$$|\boldsymbol{\jmath}_{bh}| = \cos\phi_h \tag{12}$$

where ϕ_h is a bank angle. It is not the Euler bank angle, representing the angle by which the airplane must be rotated around the body x-axis to make the wings level. Rather, it is the amount of rotation around a horizontal axis in the body x–z plane that achieves the same end. In the following we refer to ϕ_h as h-bank. In many situations, the distinction between Euler's bank ϕ and ϕ_h is not crucial. The concept of bank renders Eq. (11) more intuitive. Thus

$$\boldsymbol{W}_1 = (\boldsymbol{V}\cdot\hat{\boldsymbol{\jmath}}_b)(\boldsymbol{\jmath}_{bh}/\cos^2\phi_h) \tag{13}$$

III. Wind Extraction Filter

Equation (11) or (13) is a complete closed-form extraction of all the wind information that can be extracted at one instant. This algorithm, nevertheless, leaves something to be desired in that it is not robust. When the attitude of the airplane is such that $\phi_h = 90$ deg ($\hat{\boldsymbol{\jmath}}_b$ is vertical), the expressions fail. In the neighborhood of $\phi_h = 90$ deg, the algorithm is extremely sensitive to error. It tends to interpret small errors in the data (and, in the real world, the effect of any vertical air current) as the result of a strong horizontal wind.

It should also be kept in mind that Eqs. (11) or (13) cannot, in any case, fully determine the wind. Only the component that happens to be transverse can be determined. Extraction of the full wind must of necessity be an iterative process over a period of time during which the aircraft samples at least 90 deg of heading. We shall see in the following that it is not necessarily the best strategy to extract the transverse component all at once. For all these reasons, we define a stepwise wind extraction filter by

$$\boldsymbol{W}_{i+1} = \boldsymbol{W}_i + [(\boldsymbol{V}-\boldsymbol{W}_i)\cdot\hat{\boldsymbol{\jmath}}_b]\boldsymbol{\jmath}_{bh} \tag{14}$$

where $\boldsymbol{W}_i$ is the wind estimate for the ith step.

Note that in Eq. (14), $\cos^2\phi_h$ has been dropped. This means that, with a nonzero ϕ_h, only $W_T\cos^2\phi_h$ will be extracted in one step. However, imagine that a large number of steps can be performed while the aircraft maintains the same heading and the same ϕ_h. In that case the step-by-step extraction will yield a sequence

$$W_T(\cos^2\phi_h + \sin^2\phi_h\cos^2\phi_h + \sin^4\phi_h\cos^2\phi_h + \cdots)$$

$$= W_T\frac{\cos^2\phi_h}{1-\sin^2\phi_h} = W_T \tag{15}$$

IV. Convergence Theorem

The preceding illustration addressed the scenario where a large number of measurements could be made while a banked airplane, flying coordinated, did not change its heading appreciably. The extraction filter [Eq. (14)] is intended for use in three dimensions with the aircraft maneuvering and changing heading. The purpose is to extract the whole wind, not just a particular component. It is in this three-dimensional context that the following theorem is offered.

Theorem: The wind estimate produced by the extraction filter [Eq. (14)] approaches the true wind semimonotonically. In equation form

$$|\boldsymbol{W}_{i+1} - \boldsymbol{W}| \leq |\boldsymbol{W}_i - \boldsymbol{W}| \tag{16}$$

for all $i = 0, 1, 2, \ldots$

Proof: Subtract $\boldsymbol{W}$ from Eq. (14)

$$\boldsymbol{W}_{i+1} - \boldsymbol{W} = \boldsymbol{W}_i - \boldsymbol{W} + [(\boldsymbol{V} - \boldsymbol{W}_i)\cdot\hat{\boldsymbol{j}}_b]\boldsymbol{j}_{bh} \tag{17}$$

Note that

$$\begin{aligned}(\boldsymbol{V} - \boldsymbol{W}_i)\cdot\hat{\boldsymbol{j}}_b &= [(\boldsymbol{V} - \boldsymbol{W}) - (\boldsymbol{W}_i - \boldsymbol{W})]\cdot\hat{\boldsymbol{j}}_b \\ &= -(\boldsymbol{W}_i - \boldsymbol{W})\cdot\hat{\boldsymbol{j}}_b \\ &= -(\boldsymbol{W}_i - \boldsymbol{W})\cdot\boldsymbol{j}_{bh}\end{aligned} \tag{18}$$

The first step in Eq. (18) is straightforward algebra. The second step uses Eq. (1). The third step is based on $\boldsymbol{W}$ and $\boldsymbol{W}_i$ both being horizontal.

Substituting Eq. (18) in Eq. (17), one has

$$\boldsymbol{W}_{i+1} - \boldsymbol{W} = \boldsymbol{W}_i - \boldsymbol{W} - [(\boldsymbol{W}_i - \boldsymbol{W})\cdot\boldsymbol{j}_{bh}]\boldsymbol{j}_{bh} \tag{19}$$

Now decompose $\boldsymbol{W}_i - \boldsymbol{W}$ into two vectors, $\boldsymbol{U}_1$ along the direction of $\boldsymbol{j}_{bh}$, and $\boldsymbol{U}_2$ perpendicular to it

$$\boldsymbol{W}_i - \boldsymbol{W} = \boldsymbol{U}_1 + \boldsymbol{U}_2 \tag{20}$$

Then by Eq. (19), and using Eq. (12)

$$\boldsymbol{W}_{i+1} - \boldsymbol{W} = \boldsymbol{U}_1 + \boldsymbol{U}_2 - \cos^2\phi_h\boldsymbol{U}_1 = \sin^2\phi_h\boldsymbol{U}_1 + \boldsymbol{U}_2 \tag{21}$$

from which it follows that

$$\begin{aligned}|\boldsymbol{W}_{i+1} - \boldsymbol{W}|^2 &= \sin^4\phi_h|\boldsymbol{U}_1|^2 + |\boldsymbol{U}_2|^2 \leq |\boldsymbol{U}_1|^2 + |\boldsymbol{U}_2|^2 \\ &= |\boldsymbol{W}_i - \boldsymbol{W}|^2\end{aligned} \tag{22}$$

V. Level Turn

The convergence theorem guarantees that successive applications of the wind extraction filter never degrade the wind estimate. The goal, however, is to improve the estimate. The intention is to have the estimate converge toward the true wind. This requires that different headings be sampled.

Some insight into the workings of the filter and the strategy of applying it may be gained from a study of a level coordinated turn. The maneuver addressed has the airplane fly a circular trajectory relative to the airmass. The ground track is a cycloid. In level flight, ϕ_h becomes the wind-coordinate-system bank. In coordinated flight, ϕ_h determines the rate of turn through the universal relationship

$$\omega = (g/V)\tan\phi_h \tag{23}$$

where V is the airspeed.

We consider a level turn carried out at a constant ϕ_h and a constant V, hence at constant ω. If the filter is applied at a constant time interval of Δt, then it is applied at headings varying by $\Delta\psi = \omega\Delta t$. Δt may be restricted by the ability of computing machinery to execute the filter. However, time, as such, has no effect on the workings of the filter. It is the ϕ_h and the heading step $\Delta\psi$ that govern. In any case, we will presently see that the most frequent application of the filter that is feasible is not necessarily the optimal strategy.

For the study of the level turn, we represent the error in the estimate $\boldsymbol{W}_i - \boldsymbol{W}$ by its magnitude

$$w_i \equiv |\boldsymbol{W}_i - \boldsymbol{W}| \tag{24}$$

and by the angle γ_i that it makes with the current heading. We define γ_i to be positive to the outside of the turn (Fig. 2). Every time the filter is applied, the component of $\boldsymbol{W}_i - \boldsymbol{W}$ normal to the flight path is reduced, whereas the component along the flight path is unchanged. This means that γ_i is changed to γ_i', with

$$|\tan\gamma_i'| < |\tan\gamma_i| \tag{25}$$

However, by the next application of the filter, the aircraft has turned by $\Delta\psi$, and

$$\gamma_{i+1} = \gamma_i' + \Delta\psi \tag{26}$$

This is illustrated in Fig. 2.

The relationship between γ_{i+1} and γ_i can be made explicit. Application of the filter reduces the normal component of $\boldsymbol{W}_i - \boldsymbol{W}$ by a factor $\sin^2\phi_h$, leaving the longitudinal component unchanged. Thus

$$\tan\gamma_i' = \sin^2\phi_h\tan\gamma_i \tag{27}$$

$$\gamma_{i+1} = \arctan(\sin^2\phi_h\tan\gamma_i) + \Delta\psi \tag{28}$$

Figure 3 exhibits Eq. (28) graphically on a plot of γ_{i+1} against γ_i. Curve (a) represents $\arctan(\sin^2\phi_h\tan\gamma_i)$, and curve (b) is the identity $\gamma_{i+1} = \gamma_i$, added for reference. Curve (a) intersects curve (b) at $\gamma_i = 0$ and $\gamma_i = 90$ deg. In between, (a) lies below (b). Also note that (a) is monotonic increasing. The curve of γ_{i+1} according to Eq. (28) is obtained by translating (a) upward by an amount $\Delta\psi$. Curve (c) illustrates the result when $\Delta\psi$ is not too large. In that case, (c) intersects (b) at two points that we denote γ_{e-} and γ_{e+} ($\gamma_{e-} < \gamma_{e+}$). There is a critical value of $\Delta\psi$, $\Delta\psi_0$, at which the curve of γ_{i+1} [curve (d)] is tangent to (b) and touches it at a single point γ_0. For values of $\Delta\psi$ greater than $\Delta\psi_0$ [curve (e)], γ_{i+1} is always greater than γ_i.

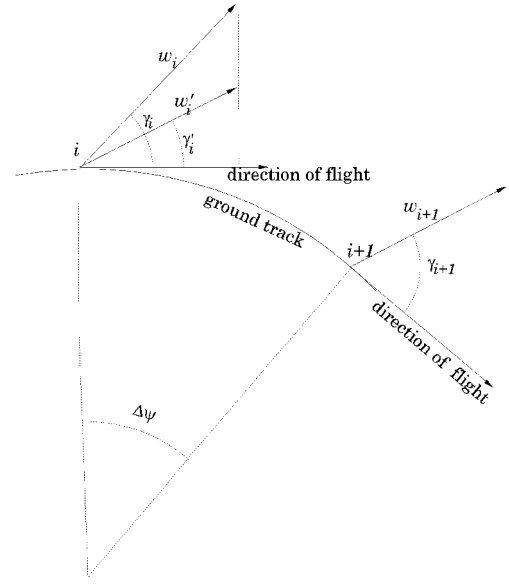

Fig. 2 Wind estimate error w at the ith and $i + 1$ updates.

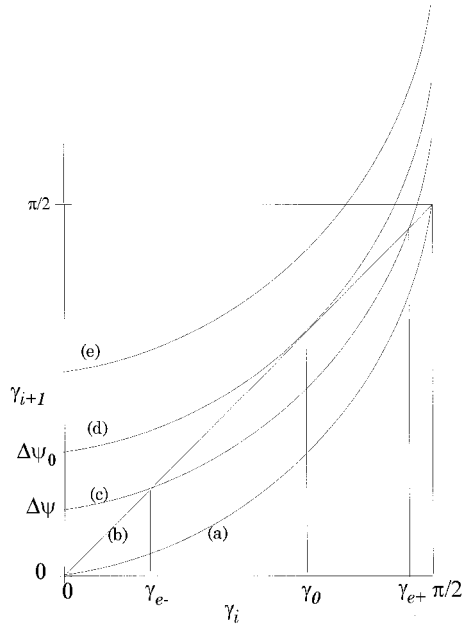

Fig. 3 γ_{i+1} vs γ_i and stationary points.

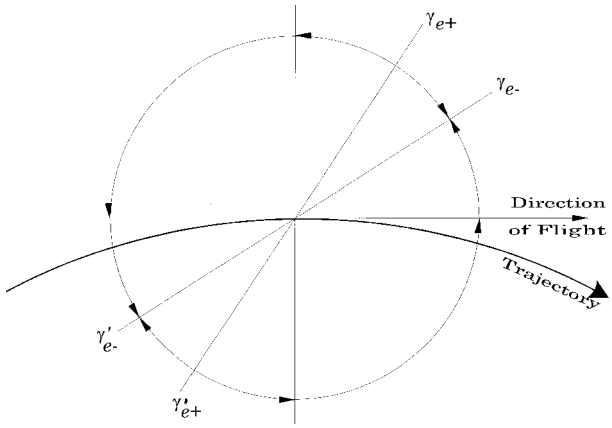

Fig. 4 Polar angle γ and its stationary points.

For subcritical $\Delta\psi$, γ_{e-} and γ_{e+} are equilibrium points at which γ_i is unchanged by application of the filter. They are both in the first quadrant. Because the period of tan γ is π, the situation in the third and fourth quadrants is a repeat of the first and second. There are two equilibrium points in the third quadrant: $\gamma'_{e-} = \gamma_{e-} + \pi$ and $\gamma'_{e+} = \gamma_{e+} + \pi$ (Fig. 4).

When the equilibrium points exist but γ_i is not at one of them, the relationship between γ_{i+1} and γ_i is

$$\begin{cases} \gamma_i < \gamma_{i+1} < \gamma_{e-} & \text{when} \quad 0 < \gamma_i < \gamma_{e-} \\ \gamma_{e-} < \gamma_{i+1} < \gamma_i & \text{when} \quad \gamma_{e-} < \gamma_i < \gamma_{e+} \\ \gamma_i < \gamma_{i+1} < \gamma'_{e-} & \text{when} \quad \gamma_{e+} < \gamma_i < \gamma'_{e-} \\ \gamma'_{e-} < \gamma_{i+1} < \gamma_i & \text{when} \quad \gamma'_{e-} < \gamma_i < \gamma'_{e+} \\ \gamma_i < \gamma_{i+1} < 2\pi + \gamma_{e-} & \text{when} \quad \gamma'_{e+} < \gamma_i < 2\pi \end{cases} \tag{29}$$

These trends are indicated by arrows in Fig. 4. They show that γ_{e-} and γ'_{e-} are stable equilibrium points. If $\gamma_i < \gamma_{e-}$, then γ_i will grow from one extraction step to the next, approaching γ_{e-} from below. If it is larger than γ_{e-} (but not larger than γ_{e+}), it will decline and tend to γ_{e-} from above. The same reasoning shows that γ_{e+} and γ'_{e+} are unstable equilibrium points that cannot be maintained. If γ_i starts above γ_{e+}, it grows through 180 deg and converges to γ'_{e-}.

We can express γ_{e-}, γ_{e+}, and $\Delta\psi_0$ in closed form. To that end, restate Eq. (28) as

$$\sin^2\phi_h \tan\gamma_i = \tan(\gamma_{i+1} - \Delta\psi) = \frac{\tan\gamma_{i+1} - \tan\Delta\psi}{1 + \tan\gamma_{i+1}\tan\Delta\psi} \tag{30}$$

This is readily solved for tan γ_{i+1} and yields

$$\tan\gamma_{i+1} = \frac{\sin^2\phi_h \tan\gamma_i + \tan\Delta\psi}{1 - \sin^2\phi_h \tan\gamma_i \tan\Delta\psi} \tag{31}$$

To find the equilibrium points, set γ_i and γ_{i+1} equal in Eq. (31). Denoting the common value by γ_e, one finds

$$\sin^2\phi_h \tan\Delta\psi\,(\tan\gamma_e)^2 - \cos^2\phi_h \tan\gamma_e + \tan\Delta\psi = 0 \tag{32}$$

which yields

$$\tan\gamma_e = \frac{1 \pm \sqrt{1 - 4\tan^2\phi_h(1 + \tan^2\phi_h)\tan^2\Delta\psi}}{2\tan^2\phi_h \tan\Delta\psi} \tag{33}$$

This equation has two real solutions, as long as $\Delta\psi$ is small enough

$$\Delta\psi < \Delta\psi_0 \equiv \arctan(\cos\phi_h/2\tan\phi_h) \tag{34}$$

Equation (33) is the closed-form expression for tan γ_{e-} and tan γ_{e+}. Equation (34) determines $\Delta\psi_0$ in the terms of ϕ_h.

It is remarkable that the preceding relationships do not involve w_i. The ratio R_i by which w_i is reduced at each step can also be determined in terms of γ_i as

$$R_i \equiv \frac{w_{i+1}}{w_i} = \frac{w'_i}{w_i} = \frac{\cos\gamma_i}{\cos\gamma'_i} = \sqrt{\frac{1 + \sin^4\phi_h \tan^2\gamma_i}{1 + \tan^2\gamma_i}}$$

$$= \sqrt{\cos^2\gamma_i + \sin^4\phi_h \sin^2\gamma_i} \tag{35}$$

As long as Eq. (34) is satisfied, γ_i will converge to γ_{e-} or γ'_{e-}. At the same time, R_i will converge to

$$R_{e-} = \sqrt{\cos^2\gamma_{e-} + \sin^4\phi_h \sin^2\gamma_{e-}} \tag{36}$$

Equation (36) is obtained from Eq. (35) by substituting γ_{e-} for γ_i. The decline of w_i becomes exponential

$$w_{i+n}/w_i = R_{e-}^n \tag{37}$$

On a logarithmic scale, this is a linear decline

$$\log w_{i+n} = \log w_i + n \log R_{e-} \tag{38}$$

Some insight might be gained from inspection of the preceding relationship in the limit of $\Delta\psi$ tending to zero, i.e., the limit of infinitely frequent applications of the filter, to the lowest order in $\Delta\psi$

$$\gamma_{e-} \approx \Delta\psi/\cos^2\phi_h \tag{39}$$

$$\log R_{e-} \approx -\frac{1 - \sin^4\phi_h}{2\,\ell n\,10\cos^4\phi_h}\Delta\psi^2 \tag{40}$$

The logarithmic slope of w_i declines as $\Delta\psi^2$, whereas the number of filter applications over a given heading interval grows only as $\Delta\psi^{-1}$. The reduction of the logarithmic error over a given heading interval declines in proportion to $\Delta\psi$ and tends to zero, even as the number of applications tends to infinity. The more frequent the applications of the filter, the less effective it becomes.

The same state of affairs prevails for finite $\Delta\psi$ with γ_i and R_i converged to γ_{e-} and R_{e-}, respectively. $|\log R_{e-}|$ increases faster than $\Delta\psi$. The benefit of the filter increases as the frequency of applying it is diminished. When $\Delta\psi$ reaches $\Delta\psi_0$, γ_{e-} becomes γ_0, defined by

$$\tan \gamma_0 = 1/\sin \phi_h \tag{41}$$

This yields

$$\cos^2\gamma_0 = \frac{\sin^2\phi_h}{1 + \sin^2\phi_h}, \qquad \sin^2\gamma_0 = \frac{1}{1 + \sin^2\phi_h} \tag{42}$$

R_{e-} becomes R_0, obtainable by substituting Eq. (42) in Eq. (36). It works out to

$$R_0 = \sin \phi_h \tag{43}$$

The situation changes drastically when $\Delta\psi$ exceeds $\Delta\psi_0$. There no longer is a stable value for γ_i. Rather, γ_i keeps increasing all the way to 2π, rolling over back to zero and over again, and sampling values in the whole range of 0–360 deg. When $\Delta\psi$ becomes much larger than $\Delta\psi_0$, one may try to estimate the average logarithmic slope of w_i vs the number of filter applications by averaging over γ_i. For ease of computation, we look at the γ average of R_i^2, which, following Eq. (35), is

$$\langle R_i^2\rangle = \tfrac{1}{2}(1 + \sin^4\phi_h) \tag{44}$$

Because the arithmetic average of two positive numbers is greater than their geometric average, one can continue

$$\langle R_i^2\rangle \geq \sin^2\phi_h = \langle R_0\rangle^2 \tag{45}$$

The last inequality suggests that once $\Delta\psi$ exceeds $\Delta\psi_0$, there are no further gains in the logarithmic slope of w_i. On the contrary, some loss may be expected. This loss is substantial for small values of ϕ_h and rather insignificant for 45 deg $\leq \phi_h \leq$ 90 deg. Even so, any further increase in $\Delta\psi$ is detrimental because of the reduction in the number of times the filter is applied over the same heading interval.

The conclusion, then, is that the wind estimate converges most rapidly when the filtering interval is chosen with $\Delta\psi$ just under $\Delta\psi_0$. In that case, once γ_i has converged to γ_0 of Eq. (41), the error in the wind estimate w_i is reduced by the factor $\sin \phi_h$ each time the filter is applied.

VI. Numerical Results

The process is illustrated in Figs. 5 and 6, which exhibit data based on Eqs. (31) and (35). The two figures show the same data. Figure 6 features a larger scale on the abcissa, making more detail visible in a smaller range. The airplane motion was simulated at a frame rate of 40 Hz (25-ms frames). The data are for an airplane performing a level turn at $\phi_h = 45$ deg. It consists of 4000 frames covering almost three complete turns. The heading change per frame comes to 0.257 deg. A wind amounting to 28.2% of the airplane's airspeed was implemented. The initial estimate of the wind was zero. The different curves in Fig. 6 represent the history of wind estimate error for different intervals of filter application expressed as a number of frames. This number varies from 10 to 1000. (In the simulation, the airspeed is about 106 kn and the windspeed is 30 kn. However, these absolute numbers are immaterial.) $\Delta\psi_0$ of Eq. (34) comes out as 19.47 deg and amounts to 75.72 frames.

Application of the filter at intervals of 10 frames, amounting to 400 iterations over the 4000 frames, reduces the wind error by a factor of about 7. Applied only once in 40 frames for a total of 100 wind updates, the filter reduces the wind error by better than 500. When the interval is increased to 70 frames, allowing only 57 updates, the improvement in wind estimate becomes of the order of 10^6.

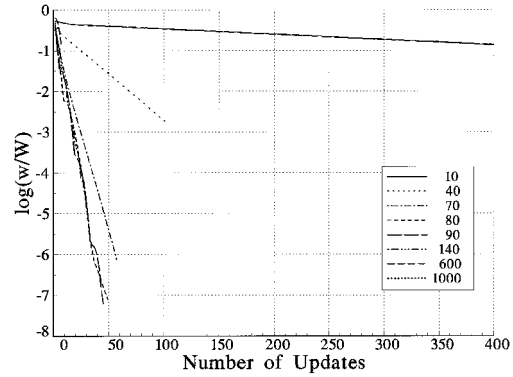

Fig. 5 Logarithmic relative error vs number of filter applications.

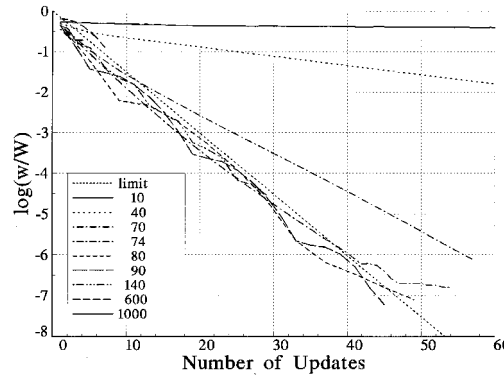

Fig. 6 Logarithmic relative error vs number of filter applications (detailed view), with limit slope log R_0 shown for reference.

$\Delta\psi_0$ is crossed around 75. The 74 curve has a slope close to the critical slope log R_0, which is shown for reference in Fig. 6, and achieves an improvement by a factor just short of 10^7. The 80 and 90 curves actually exceed 10^7. The 74 frame curve and the 80 and 90 frame curves interweave and have comparable slopes, as do all curves for longer update intervals. All of these curves cluster just below the limit curve. Among these curves, more frequent updates (longer curves) produce the more accurate wind estimates. The rule of thumb that best estimates are produced near the critical update interval is confirmed.

VII. Conclusions

We defined a wind extraction filter (Sec. III) and showed that it produces wind estimates that monotonically approach the true wind (the convergence theorem, Sec. IV). The assumptions concerning the wind were that it was horizontal and constant in both space and time. The assumptions concerning the flight were that it was coordinated.

Only the transverse component of the wind is addressed when the filter is applied, and a single application recovers only a fraction $\cos^2\phi_h$ of the transverse error. Repeated applications, while the aircraft changes heading, can produce a wind estimate as accurate as one wishes. Study of a level turn showed, however, that the rate at which the wind estimate converges to the true wind depends on the heading interval at which the filter is applied. The fastest convergence occurs when the filter is applied at heading intervals equal to $\Delta\psi_0$, which depends on ϕ_h.

The numerical results of the last section were obtained in a steady coordinated level turn. It is important to examine the

conditions actually used in the analytic derivation in Sec. V. The derivation depended on ϕ_h and $\Delta\psi$ being constant.

The last assumption does not appear essential. Obviously, it would be best to apply the filter when $\gamma = 90$ or 270 deg, which would assure a convergence ratio R_i equal to $\sin^2\phi_h$. However, the wind estimate error, and with it γ, are unknown. Using an update heading interval just under $\Delta\psi_0$ guarantees $\gamma = \gamma_0$, and $R_i = \sin\phi_h$. It was shown that this was better than the γ average, and there does not seem to be a way to guarantee better convergence.

The h-bank may vary during maneuvering. If the h-bank varies slowly, a sequence of wind updates adjusted for the current h-bank will adiabatically track the situation and provide optimal convergence. We therefore recommend that each wind update be delayed until the heading increment from the last update reaches $\Delta\psi_0$ based on the current ϕ_h, or until an arbitrarily imposed time-out period has expired, whichever comes first. The $\Delta\psi_0$ rule safeguards against slow convergence resulting from a filter application rate that is too rapid. The time-out period ensures that periodic updates do occur during long legs of straight flight to account for changes in the wind over place and time.

Application of this rule in the computer simulation described in Refs. 2 and 5 leads to fast convergence to the correct wind and efficient operation of the K&G prediction methods.

Acknowledgments

This work was supported in part by the U.S. Army Simulation, Training and Instrumentation Command under Subcontract N61339-91-D-0001 and in part by U.S. Army Research Institute under ASI-97-KDC-1058-13; Subcontract under MDA903-93-C-0161.

References

[1]"IEEE Standard for Information Technology—Protocols for Distributed Interactive Simulation Applications," Inst. of Electrical and Electronic Engineers, Std. 1278-1993, New York, May 1993.

[2]Rope, A. R., "The SIMNET Network and Protocols," Bolt Beranek and Neuman Systems and Technologies, Rept. 7102, prepared for the Defense Advanced Research Projects Agency, Cambridge, MA, July 1989.

[3]Katz, A., "Event Correlation for Networked Simulators," *Journal of Aircraft*, Vol. 32, No. 3, 1995, pp. 515–519.

[4]Katz, A., Sharma, M., and Wahrenberger, D. E., "Advanced Dead Reckoning and Smoothing Algorithms," U.S. Army STRICOM Contract N61339-91-D-0001, Architecture and Standards, Delivery Order 0035, CDRL A030, Orlando, FL, May 25, 1996.

[5]Katz, A., and Graham, K., "Extrapolation of Airplane Flight," Univ. of Alabama Flight Dynamics Lab., Rept. 93S03, Dec. 19, 1993, prepared for Loral Western Development Labs, San Jose, CA, under Subcontract SO-242825-A, item 04.

[6]Katz, A., and Graham, K., "Prediction of Airplane States," *Journal of Aircraft*, Vol. 32, No. 3, 1995, pp. 563–569.